Quantum chaos in a ripple billiard

Wenjun Li,[1,2] L. E. Reichl,[1,2] and Biao Wu[2]
[1]*Center for Studies in Statistical Mechanics and Complex Systems, The University of Texas at Austin, Texas 78712*
[2]*Department of Physics, The University of Texas at Austin, Austin, Texas 78712*
(Received 18 July 2001; published 21 May 2002)

We study the quantum chaos of a ripple billiard that has sinusoidal walls. We show that this type of ripple billiard has a Hamiltonian matrix that can be found exactly in terms of elementary functions. This feature greatly improves computation efficiency; a complete set of eigenstates from the ground state up to the 10 000th level can be calculated simultaneously. Nearest neighbor spacing of energy levels of a chaotic ripple billiard shows a Brody distribution (with a confidence level of 99% by χ^2 test) instead of the Gaussian orthogonal ensemble prediction. For high energy levels we observe scars and interesting patterns that have no resemblance to classical periodic orbits. Momentum localization of scarred eigenstates is also observed. We compare the scar associated localization with quantum dynamical Anderson localization by drawing the wave function distribution on basis state coefficients.

DOI: 10.1103/PhysRevE.65.056220 PACS number(s): 05.45.Mt, 05.30.−d, 73.20.−r

I. INTRODUCTION

The search for the signatures of chaos in atomic and mesoscopic systems has attracted increasing interest in recent years [1–11] because underlying classical chaos appears to give rise to universal behavior of many quantum systems. Recently, billiards of arbitrary shape have been created with lasers and cold atoms, and this opens a new testing ground for such systems [12].

One of the most studied properties for bounded quantum systems is the statistics of the distribution of nearest neighbor energy level spacings. This statistics appears to depend only on general space-time symmetries [6–10] if the underlying classical dynamics is chaotic. However, many of the systems studied so far, experimentally or numerically, have insufficient data on energy levels to determine the distribution of level spacings with a large confidence level [8].

In this paper, we study properties of the ripple billiard, one or two of whose walls are sinusoidal (see Fig. 1). As the amplitude of the ripple is increased, its classical dynamics transits from integrable, to mixed, to fully chaotic, and then to mixed behavior again. As we shall show, the ripple billiard has a very useful feature that the elements of its Hamiltonian matrix can be obtained analytically in terms of elementary functions. This greatly increases the computation efficiency, and allows us to obtain up to 10 000 contiguous eigenstates (approximately an order of magnitude higher than many chaotic systems studied to date). This large number of energy levels will allow us to examine the spectral statistics with greater confidence level than has been possible in most previous studies.

For a spinless particle in a two-dimensional chaotic billiard with time-reversal symmetry, the distribution of nearest neighbor level spacings (with spatial parities separated) is expected to obey approximately a Wigner distribution, or more precisely, the prediction of the Gaussian orthogonal ensemble (GOE) [13] that gives a Brody distribution function

$$P(s)=A\frac{a}{D}s^{\beta}\exp\left(-\frac{a}{D}s^{1+\beta}\right), \tag{1}$$

with a Brody parameter $\beta=0.953$, instead of $\beta=1.0$ as given by Wigner distribution. In Eq. (1), D is the mean level spacing and $A=a(1+\beta)$ and $a=[\Gamma(2+\beta)/(2+\beta)]^{1+\beta}$.

As was pointed out by Graf *et al.* [9], in a real quantum chaotic system like a billiard, the existence of marginally stable "bouncing ball states" [9] can destroy the fit to the GOE prediction. As will be shown in this paper, this can be seen best by using a χ^2 test [14] that tells us quantitatively how well a given set of data fits an expected distribution.

Scars are considered to be one of the most surprising properties of quantum systems whose underlying classical dynamics is chaotic. An experimental observation of such an effect in a true quantum system has long been considered as a conceptual breakthrough [11]. In the ripple billiard system considered here, the fact that we have an analytic expression for the Hamiltonian matrix allows us to investigate scar wave functions and properties up to very high energy levels. Beside the well known feature of scarred wave functions that resemble a classical particle traveling along periodic orbits, we notice that scarred states also show other classical behav-

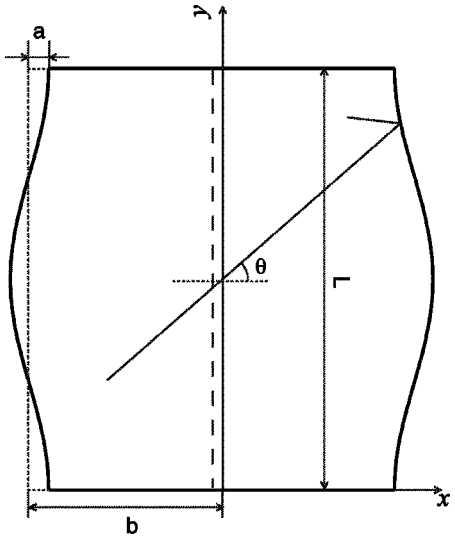

FIG. 1. Ripple billiard.

iors. From Husimi plots [5] and analysis in two-dimensional momentum space, strong localization of the momentum distribution for a scarred eigenstate is observed.

We compare the scar associated localization with the well-known quantum dynamical Anderson localization, which has been observed in many quantum chaotic systems such as a δ-kicked rotor [12] and various types of billiards [15,16]. We notice that they are two different types of localizations. Quantum dynamical localization basically corresponds to a regime among all energy levels (above the perturbative regime yet below the ergodic regime), while the scar associated localization corresponds to that particular scarred eigenstate. We will make this clear by drawing the wave function distribution on basis coefficients.

Interference between different scarred orbits is also observed in wave functions of the ripple billiard, and may even form new wave function patterns, such as the hexagon and circle-like structures shown in this paper.

The calculation of the Hamiltonian matrix of the ripple billiard will be given in the Appendices. In Sec. II, we introduce the ripple billiard model. In Sec. III, we examine the statistical properties of the energy eigenvalues. In Sec. IV, we analyze scarred eigenstates and associated localizations. Section V shows some pattern formations in the ripple billiard. Finally in Sec. VI, we make some concluding remarks.

II. RIPPLE BILLIARD MODEL

The right wall of the ripple billiard, shown in Fig. 1, has the form

$$f(y)=b-a\cos\left(\frac{2\pi y}{L}\right), \tag{2}$$

where a is the ripple amplitude in units of the ripple height L_0. The height $L=1.0$ in this paper (see Appendix A for a discussion of units). When $a=0$, the billiard is a rectangle with width $2b$ (similarly, in units of L_0). Classically, as the ripple amplitude a increases from zero, the ripple billiard changes from an integrable system to a mixed, and then to a fully chaotic system, and for very large a it becomes mixed again. This can be illustrated easily by drawing the Poincare surface of section when considering a classical particle colliding with the billiard boundaries.

III. ENERGY LEVEL STATISTICS

Although a direct counterpart of the classical Poincare surface of section is not available quantum mechanically, depending on the degree of chaos in the underlying classical dynamics, quantum systems do show different features. Among them the energy level statistics has been studied most extensively. Nowadays the universal statistical properties have been widely accepted as important signatures of quantum chaos, and this has been verified in experiments [9–11,17] as well as various numerical simulations [8–10].

However, due to the limited number of available eigenstates, in many cases the data can only show a qualitative agreement with the random matrix theory (RMT) prediction, while quantitative comparison according to a χ^2 test [14] generally does not give a satisfying confidence level [8]. In addition, other factors affecting the dynamics of a chaotic system may also cause deviations from GOE predictions. One example, as shown by Graf *et al.* in a quarter stadium billiard, is the existence of so called bouncing ball states, whose wave functions resemble a particle bouncing perpendicularly off the straight sections of the billiard [9], may cause the deviation of nearest neighbor level spacings from RMT behavior. Here with our ripple billiard we can examine this effect quantitatively. We find that the types of states having the greatest affect on the statistics for the ripple billiard are the vertically concentrated eigenstates (associated with a vertical marginally stable orbit) and the horizontally concentrated eigenstates (associated with a horizontal stable orbit). Figure 2(a) shows the distribution of nearest neighbor spacings for 1000 eigenstates (corresponding to the levels between 1000th and 2000th levels). The distribution looks basically ''GOE-like'' but comparison with the GOE prediction (the solid curve in the figure) gives $\chi^2_{17}=16.03$, corresponding to a low confidence level of 45.11%. If we extract the vertical bouncing ball states (based on a Bohr-Sommerfeld-like quantization criteria [18]), the new distribution has $\chi^2_{17}=10.92$ and the confidence level increases to 81.44%. If we further extract the horizontal states [both are sketched in the inset of Fig. 2(b)], the confidence level increases dramatically to 99.08%, as shown in Fig. 2(b).

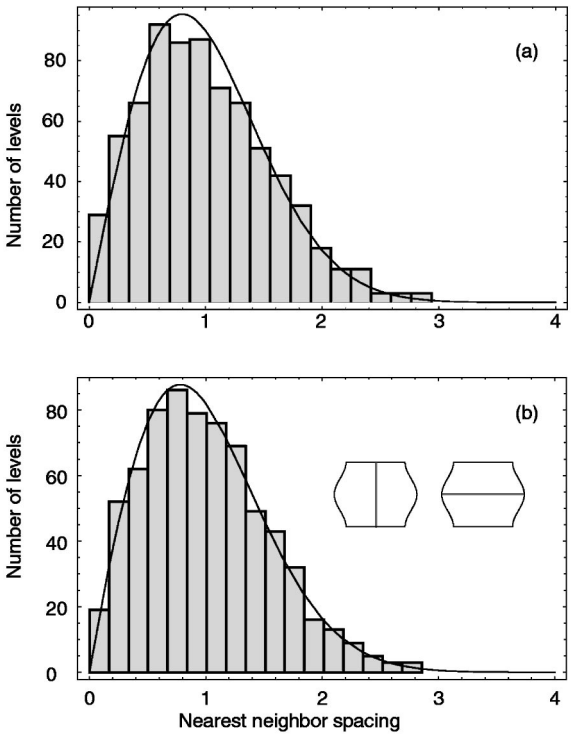

FIG. 2. (a) χ^2 test of the GOE prediction (the solid curve is the Brody distribution for $\beta=0.953$) for the 1000th–2000th levels. $\chi^2_{17}=16.03$ corresponds to a low confidence level of 45.11%. (b) With vertically and horizontally concentrated states (sketched in the inset) extracted. $\chi^2_{17}=5.73$, and the confidence level is 99.08%. Even-even modes are used and $a=0.05$, $b=0.5$.

Instead of the GOE prediction, Graf *et al.* also pointed out

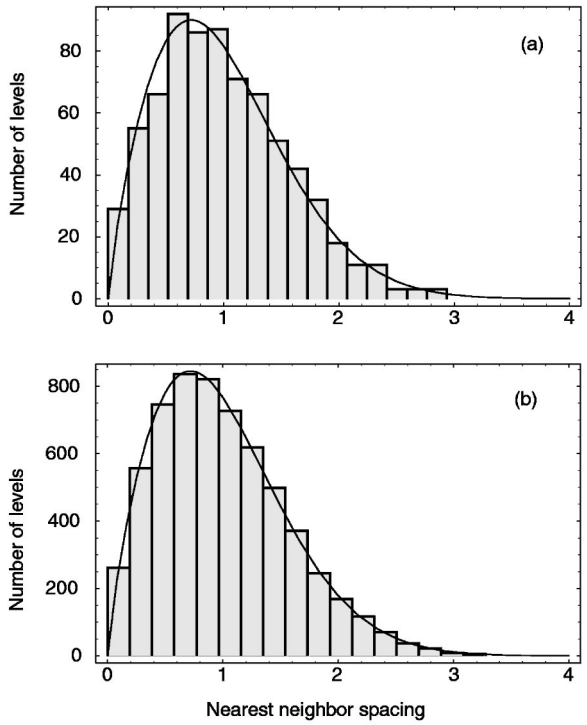

FIG. 3. χ^2 test of the Brody distribution with Brody parameter of 0.806. (a) The statistics of 1000 eigenstates gives $\chi^2_{17}=7.47$ (corresponding to a confidence level of 96.30%); (b) the statistics of 7000 states gives $\chi^2_{17}=5.00$ (corresponding to a confidence level of 99.58%).

[9] that the full distribution of nearest neighbor spacings (without states extraction) of a quarter stadium billiard can be best fitted by a Brody distribution [1] with Brody parameter much less than 1.0. This claim can also be examined for our ripple billiard with a χ^2 test. For the 1000 eigenstates mentioned above, the distribution of nearest neighbor spacings agrees with the Brody distribution (by choosing Brody parameter β of 0.806) with a good confidence level of 96.30% [Fig. 3(a)]. Since the Hamiltonian matrix of our ripple billiard can be obtained analytically, we extended our matrix size to 10 000 and did the statistics using the first 7 000 levels above the ground state (to guarantee the accuracy of energy eigenvalues obtained), the distribution of nearest neighbor level spacings shows an excellent agreement with the Brody distribution [Fig. 3(b)], where the confidence level is 99.58%.

In our calculations here we separated the parities. The data used in Figs. 2 and 3 are even-even modes. The eigenenergies were unfolded using the same method as applied in Ref. [17]. The transform of the original energy spectrum $\{E_i\}$ to the unfolded spectrum $\{\overline{E_i}\}$ can be written

$$\overline{E}_{i+1}=\overline{E}_i+(2\ell+1)\frac{E_{i+1}-E_i}{E_{j_2+1}-E_{j_1}}, \tag{3}$$

$$j_1=\max(1,i-\ell), \quad j_2=\min(n-1,i+\ell).$$

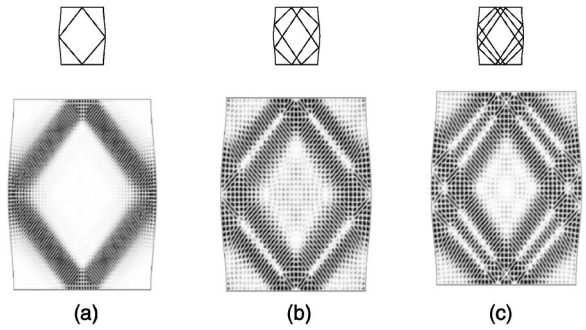

FIG. 4. Plots of three energy eigenstates that are scarred. Corresponding periodic orbits are plotted above. (a) The 1028th state, (b) 531st state, and (c) 539th state. (b) involves one orbit and its horizontal reflection, while (c) involves three separate orbits, in fact, they are the superpositions of the orbits from (a) and (b). Parameters are $b=0.5$, $a=0.02$; even-even modes are used.

The parameter ℓ we used is 137 for 1 000 levels, and 442 for 7 000 levels, respectively.

IV. SCARS

One of the most interesting phenomenon that occurs in quantum chaotic systems is the observation of scars. For scarred eigenstates, the probability amplitude of an eigenstate is concentrated along unstable periodic orbits instead of being randomly distributed in the cavity [20,23]. Scars were originally observed by McDonald [19] for numerical simulations of a stadium billiard (which is now considered as a paradigm model in quantum chaology) but did not catch much attention until the extensive studies of Heller [4]. We are going to see in this section some new features in our ripple billiard by examining the scarred states. As seen in Fig. 4, the probability densities of some eigenstates are enhanced along the path of classical periodic orbits. These scar patterns look quite ''clean'' (the probabilities in regions other than the orbits are fairly low). The scarring pattern in each of the states in Fig. 4 is not limited to that particular eigenstate; instead it reappears again and again as energy increases.

Besides wave function enhancement along classical periodic orbits, scarred states show other classical behaviors. Below we compare the Husimi plot [21,22] of a scarred state with its classical Poincare surface of section. The Poincare section [the position axis is chosen as the dashed line as shown in Fig. 5(a), which has a small shift from the central vertical line] in this case consists of two dots as shown in Fig. 5(b). This agrees well with the quantum Husimi plot as shown in Fig. 5(c). (For the Husimi plots, the position coordinates as defined in the Husimi function are also chosen along the dashed line in Fig. 5(a). A more detailed description for making the Husimi plots is given in Appendix B.)

To further investigate the scarred eigenstate, we do an analysis of the wave function distribution in two-dimensional momentum space. In Fig. 6, we find the momentum distribution for this scarred state is highly localized in four small regions. Now if we view the energy of the quantum eigenstate, E_q, as the energy of a classical particle, E_c, the magnitude of momentum $|P|$ of the particle is then $\sqrt{E_c}$ (in units

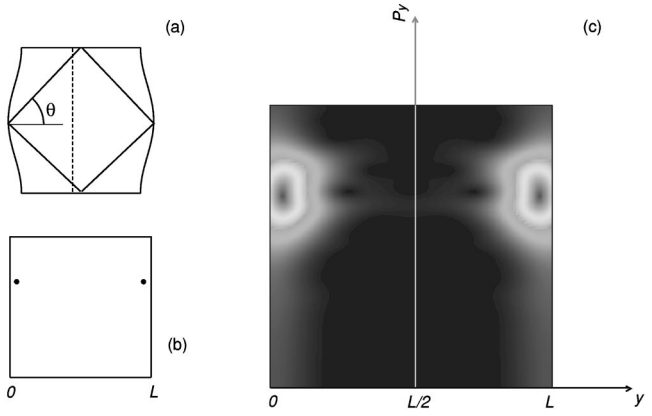

FIG. 5. The Husimi plot of the scarred state of Fig. 4(a). (a) is a corresponding classical ripple billiard, and (b) shows the Poincare surface of section [with the dashed line in (a) as the coordinate axis] associated with this periodic orbit, which in this case includes only two dots. Plot range for the coordinate is from 0 to L, and for the conjugate momentum is from 0 to $\sqrt{E}$. The eigenenergy E for this scarred state is 5228.87 (in units of $\pi^2\hbar^2/2m_eL_0^2$).

of $\hbar/L_0$). The path of this periodic orbit makes an angle θ with respect to the horizontal axis [see Fig. 5(a)]. The x and y components of momentum are $\pm|P|\cos\theta$ and $\pm|P|\sin\theta$, respectively. The momentum values derived *classically* in this way match exactly with those for the quantum momentum localizations in Fig. 6. This correspondence illustrates the *classical particle feature* of scarred states.

A. Quantum dynamical Anderson localization

From the above momentum localization of scarred states, it is natural to ask whether this localization is related to quantum dynamical localization (dynamical Anderson localization). Quantum dynamical localization shows a fundamental difference between classical and quantum mechanics. This can be seen from the diffusion behavior. For example,

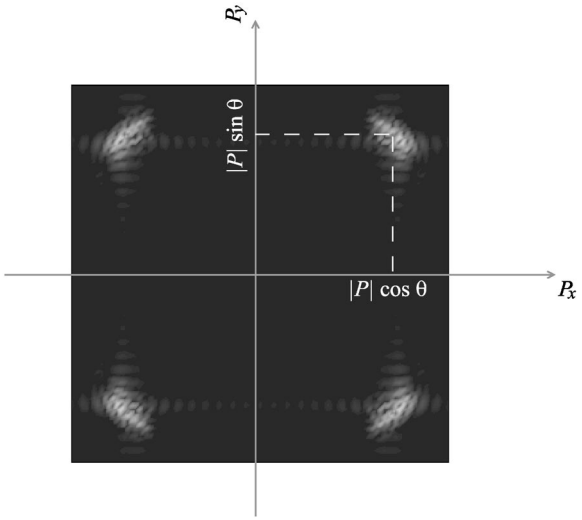

FIG. 6. Momentum localization of the scarred eigenstate in Fig. 4(a). The locations of the four small regions can be classically predicted. Plot range is from $-\sqrt{E}$ to $\sqrt{E}$ in both directions.

for a classical chaotic δ-kicked rotor [12], the change of energy with respect to the number of kicks behaves diffusively. However, for the quantum counterpart of this system, energy diffusion is suppressed due to quantum interference between eigenstates, and a wave function can be localized on some basis states as observed numerically [1] and experimentally [12]. This is known as quantum dynamical localization, or dynamical Anderson localization due to its analogy to the Anderson localization in disordered systems.

Quantum dynamical localization was also observed in billiard systems, for example, in a chaotic Bunimovich stadium billiard [15] and circular billiard with rough boundaries [16]. The energy levels from low to high energies can be divided into three regimes, namely, perturbative, localized, and ergodic, respectively. In the ergodic regime, a wave function has its support almost homogeneously on all basis states (in both billiard cases studied [15,16], the angular momentum basis was used). In the localized regime, the wave function distribution is generally logarithmically localized on the basis states. The location of the three regimes depends on the billiard parameters. A given energy eigenstate, which is known to be ergodic at parameter, say a_1, may fall into the localized regime at a smaller parameter a_2 (eventhough a_2 also corresponds to full chaos classically).

For our ripple billiard, instead of choosing angular momentum states as the expansion basis, we are going to introduce a different approach that is very suitable for the ripple billiard. As shown in great detail in the Appendices, we make a coordinate transformation which can convert the ripple billiard into a rectangular billiard [from real (x,y) space to (u,v) space] . In the rectangular (u,v) billiard, the ℓth eigenstate wave function can be written as

$$\phi_\ell = \sum_{m=1}^{\infty}\sum_{n=1}^{\infty} B_{mn}^{\ell}\varphi_{mn}(u,v), \tag{4}$$

where the functions $\varphi_{mn}(u,v)$ are for an orthonormal basis [see Eq. (A6)]. In this basis, we can see quantum dynamical localization in the ripple billiard. For any ripple amplitude a, the wave function distribution on basis coefficients B_{mn} becomes increasingly homogeneous for high energy levels.

It is interesting to note that in two-dimensional (m,n) space, the distribution of B_{mn} is mainly concentrated along a curve, where the basis states φ_{mn} with (m,n) values on the curve have the same energy as that eigenstate. This curve approximately satisfies the equation,

$$m^2+n^2=E,$$

where E is the energy. This equation defines a quarter of a circle with positive m's and n's [in the discussion below we will use angle α to denote the point (m,n), with $\tan\alpha = n/m$].

Figure 7 shows the distribution of values of B_{mn} along this quarter circle for the 1028th eigenstate for $a=0.09$ and 0.02. It clearly shows that for $a=0.09$, the distribution of values of B_{mn} is roughly homogeneous (in the ergodic regime for this a), while for $a=0.02$, it is logarithmically localized (in the localized regime for this a).

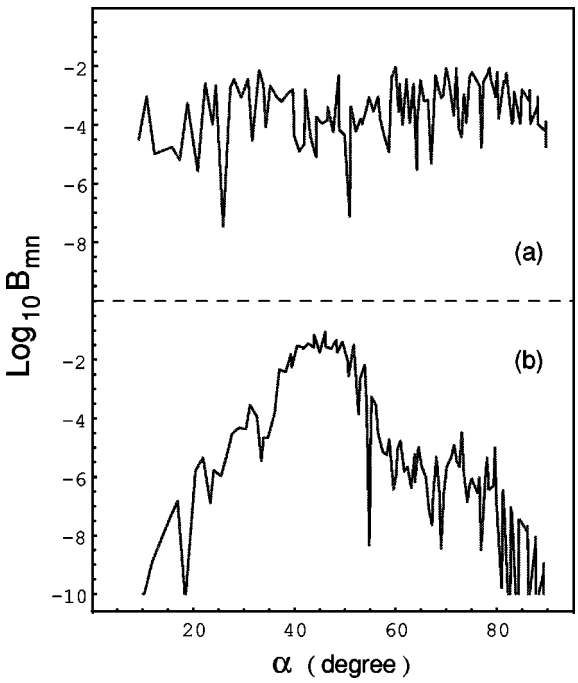

FIG. 7. Comparison of basis coefficient distribution for the 1028th eigenstate. B_{mn} is the wave function coefficient, with m, n characterizing the basis state in the transformed (u,v) box as described in text. Angle α measures the (m,n) values, $\tan\alpha = n/m$. (a) ergodic case with ripple amplitude $a = 0.09$, (b) localized case with $a = 0.02$. Other parameters are same as in Fig. 4.

B. Scarring localization

In Fig. 6 we saw that the scarred 1028th eigenstate was localized in momentum. The localization associated with scars is different from the dynamical localization discussed in the preceding section. It holds for single isolated eigenstates, while dynamical localization occurs on a continuous range of energy levels, no matter if they are scarred or not.

Below we show the localization associated with a scar by drawing the distribution of B_{mn} in two-dimensional basis state coefficient space. We compare the scarred 1028th eigenstate [see Fig. 4(a)] and an unscarred (the 1025th) eigenstate, whose wave function looks quite random (see Fig. 8). Figure 9 shows the distribution of B_{mn} for the 1025th eigenstate. In this figure, we do not plot values of B_{mn} that are less than 10^{-10}. In Fig. 9, as we just mentioned in the preceding section, the coefficients are distributed mainly along the "quarter circle." Here it is marked by *B*. Starting from the points on curve *B*, there are also many *tails* extending outward. We denote these tails by *A*.

Now we take a look at the nearby 1028th scarred eigenstates [Fig. 4(a)]. In Fig. 10 we again see that the coefficients are mainly distributed along the quarter circle *B* and we see also the tail lines *A*. They roughly cross at a point, say *O*. Nevertheless, the distribution, in particular for the tail lines, is much more narrowed (more closely localized to point *O*). The location of *O* can be easily understood. Its associated basis state (with this specific *m* and *n* value) corresponds to an ideal particle moving along a path that the scarred state follows as shown in Fig. 4(a). Since the scarring pattern is not really a geometry path, the coefficient distribution is not an isolated peak at *O*.

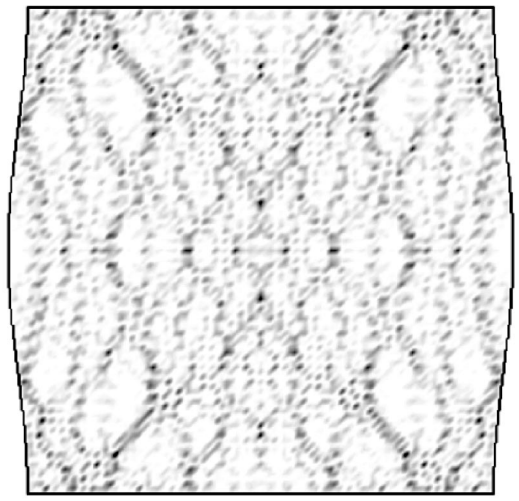

FIG. 8. The 1025th eigenstate as an example of an unscarred eigenstate. Same parameters as Fig. 4.

Comparing Figs. 9 and 10, we find that a more localized distribution of B_{mn} in two-dimensional coefficient space implies the existence of scarring effect in coordinate space. This feature is verified for other energy levels as well. Like in the coordinate space a scarring pattern can repeat itself as the energy changes, the corresponding localization behavior of B_{mn} distribution also reappears as expected.

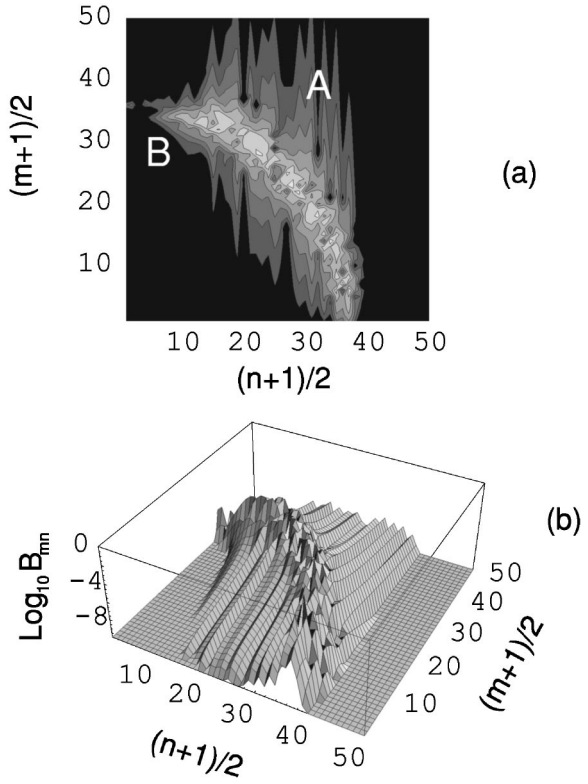

FIG. 9. The basis coefficient distribution for the unscarred 1025th eigenstate.

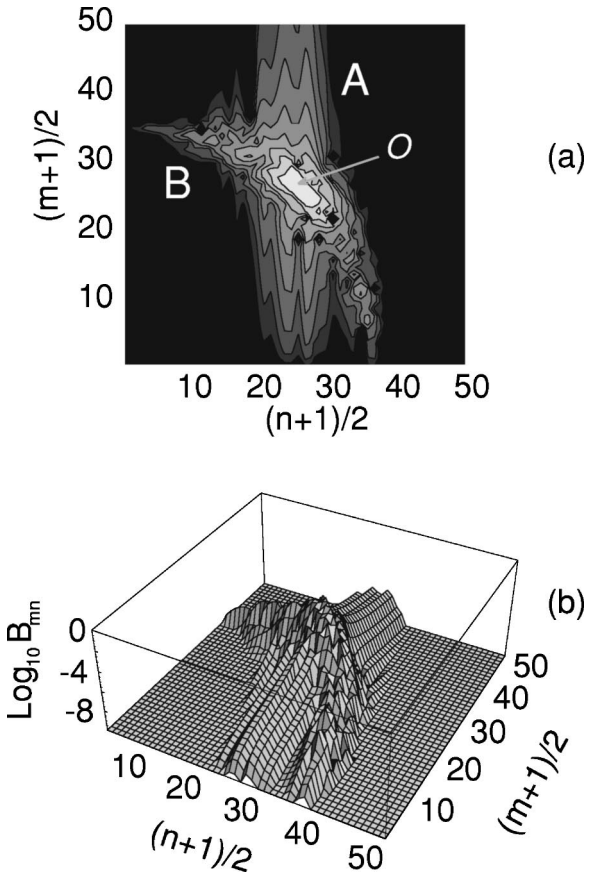

FIG. 10. The basis coefficient localization for the scarred 1028th eigenstate [Fig. 4(a)]. The central peak is at point O, which has (m,n) values that correspond to a classical particle carrying the energy of this eigenstate and undergoing the scarring orbit.

V. PATTERN FORMATION

The scarred state shown in Figs. 4(c) involves the superposition of orbits in Figs. 4(a) and 4(b). The superposition and interference of multiple scar orbits can result in new patterns that may not seem to follow a classical orbit, like the hexagon pattern shown in Fig. 11. The vertical and horizontal orbits interact when they cross each other and organize themselves to form a local hexagon structure. (In this figure, in order to better show this pattern, we extend the ripple length and show one half of the wave function. The Hamiltonian matrix can be derived similarly with slight modifications.) This pattern also repeats itself as we vary the energy. If we change the shape of our ripple by a small amount, this pattern still remains robust. For example, Fig. 11 is the 554th eigenstates for $a=0.05$, and we find that the 554th eigenstate for $a=0.045$ and $a=0.0475$ also have the same hexagon pattern. For $a=0.0525$, this pattern shifts in energy to the 562nd eigenstate, while for $a=0.0550$, the 544th eigenstate shows this pattern.

It is interesting that this hexagon structure looks quite similar to the pattern formation in classical dissipative nonlinear systems [24], eventhough their underlying mechanics are totally different. In the classical experiments [24], besides the hexagon structure, another fundamental pattern observed was circles. In fact we also find circlelike patterns in our ripple billiard, such as the example shown in Fig. 12.

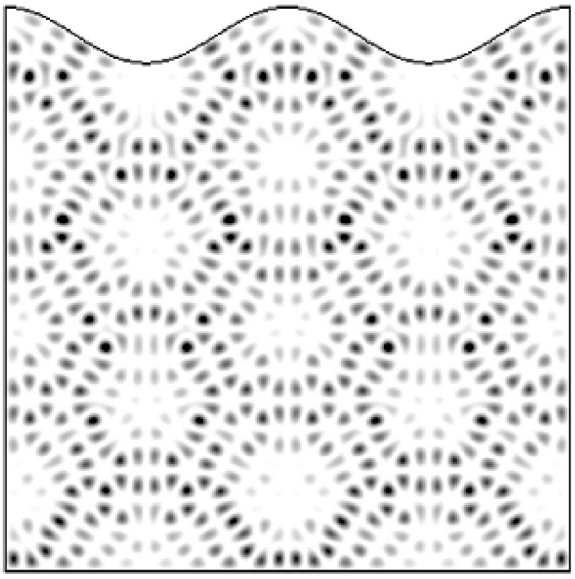

FIG. 11. Hexagon pattern formation in a ripple billiard. Ripple magnitude a is 0.05 and $b=1.0$. The ripple length is doubled and only one half of the wave function is plotted. This is the 554th eigenstate (odd-odd modes are used).

VI. CONCLUSIONS

In this paper, we have shown that a ripple billiard has an analytic Hamiltonian matrix and this fact assists us in obtaining a complete set and large number of eigenstates for statistical studies as well as in looking for features associated with very high energies, such as the scarring effect and the correspondence between quantum and classical systems. Our numerical results show clearly the deviation of nearest

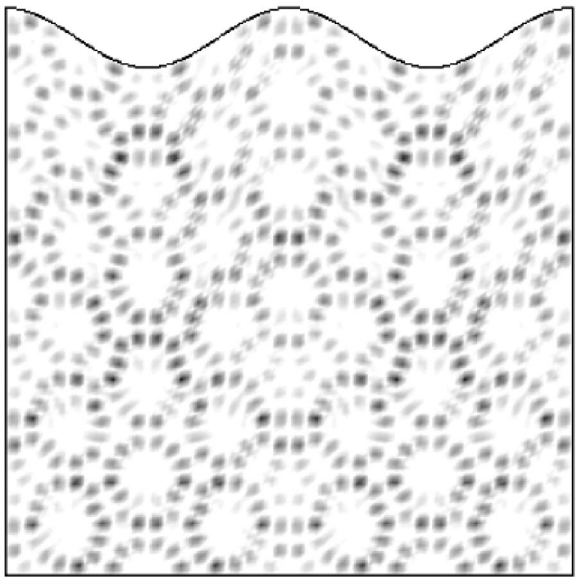

FIG. 12. Circlelike pattern formation in a ripple billiard. Same parameters as in Fig. 11 except $a=0.0525$. This is the 546th eigenstate.

neighbor spacings of energy eigenvalues of a chaotic ripple billiard from the GOE prediction. According to the Husimi plots and analysis in two-dimensional momentum space, a strong momentum localization is observed for a scarred state. We compare the localization behavior of a scar with quantum dynamical Anderson localization, by analyzing the wave function distribution on a basis set. We also show two typical patterns in the ripple billiard eigenstates, the hexagon and the circlelike structures.

ACKNOWLEDGMENTS

The authors wish to acknowledge the Welch Foundation Grant No. F-1051, NSF Grant No. INT-9602971, and DOE Contract No. DE-FG03-94ER14405 for partial support of this work. We also thank the University of Texas at Austin High Performance Computing Center for the use of their computer facilities. We thank Gursoy Akguc for helpful discussions.

APPENDIX A: THE HAMILTONIAN MATRIX FOR THE RIPPLE BILLIARD

The stationary Schrödinger equation of a two-dimensional billiard is

$$-\frac{\hbar^2}{2m_e}\left(\frac{\partial^2}{\partial x^2}+\frac{\partial^2}{\partial y^2}\right)\psi_n(x,y)=E_n\psi_n(x,y), \tag{A1}$$

where the wave function $\psi_n(x,y)$ vanishes on the walls of the billiard (shown in Fig. 1). The difficulty in solving Eq. (A1) lies in how to deal with the curved boundaries that control all the physics of the billiard. Our method is to straighten the boundaries with a coordinate transformation [5,6], then expand ψ_n in terms of a chosen basis that satisfies the boundary condition automatically.

The Schrödinger equation (A1) can be made unitless by choosing units as follows; length is taken in units of L_0 (the height of the billiard has to be specified) so that $x=x'L_0$ and energy in units of e_0, so that $E_n=E_n'e_0$, where $e_0=\hbar^2/2m_eL_0^2$. For example, if $L_0=61.7$ nm, the units of energy $e_0=0.01$ meV. Equation (A1) then becomes

$$-\left(\frac{\partial^2}{\partial x'^2}+\frac{\partial^2}{\partial y'^2}\right)\psi_n(x,y)=E_n'\psi_n(x,y). \tag{A2}$$

The energy units used in the figures of this paper, in fact, have an additional multiplying factor of π^2 for the convenience of computing. In the subsequent equations we drop the superscript $(')$ from x', y', and E_n'.

The straightening of the boundaries is done by introducing a pair of curvilinear coordinates (u, v) with

$$u=\frac{x}{2f(y)}, \quad v=y. \tag{A3}$$

In terms of coordinates (u,v), the ripple billiard is turned into a square billiard, and the Schrödinger equation becomes

$$-\left(h_1\frac{\partial^2}{\partial u^2}+h_2\frac{\partial^2}{\partial u\partial v}+h_3\frac{\partial}{\partial u}+\frac{\partial^2}{\partial v^2}\right)\phi_n(u,v)=E_n\phi_n(u,v), \tag{A4}$$

where

$$h_1=\frac{1}{4f^2}+\left(\frac{f'}{f}\right)^2u^2,$$

$$h_2=-\frac{2f'}{f}u,$$

$$h_3=2\left(\frac{f'}{f}\right)^2u-\frac{f''}{f}u. \tag{A5}$$

Equation (A4) can be viewed as the Schrödinger equation in a curved space. In other words, the ripple billiard is equivalent to a square billiard in a curved space.

The choice of the basis states is now obvious; they are

$$\varphi_{mn}(u,v)=\sqrt{\frac{2}{f(v)}}\sin\left[m\pi\left(u+\frac{1}{2}\right)\right]\sin(n\pi v), \tag{A6}$$

which automatically satisfy the boundary conditions at $u=\pm 1/2$, $v=0,1$. It is easy to verify that they obey the following orthonormal relation,

$$\int\int\varphi_{mn}^*(u,v)\varphi_{mn}(u,v)\frac{\partial(x,y)}{\partial(u,v)}dudv=\delta_{mm'}\delta_{nn'}, \tag{A7}$$

where

$$\frac{\partial(x,y)}{\partial(u,v)}=2f(v). \tag{A8}$$

With the expansion

$$\phi_\ell=\sum_{m=1}^{\infty}\sum_{n=1}^{\infty}B_{mn}^{\ell}\varphi_{mn}(u,v), \tag{A9}$$

Eq. (A4) is transformed to a matrix problem,

$$\sum_{m=1}^{\infty}\sum_{n=1}^{\infty}H_{mnm'n'}B_{m'n'}^{\ell}=E_\ell B_{mn}^{\ell}, \tag{A10}$$

where the Hamiltonian matrix includes four parts

$$H=H_0+H_1+H_2+H_3. \tag{A11}$$

Their matrix elements are

$$(H_0)_{m'n'mn}=\delta_{m'm}\left(n^2\pi^2\delta_{n'n}-\frac{1}{4}J^5_{n'n}-\frac{n'\pi}{2}J^2_{n'n}+\frac{n\pi}{2}J^2_{n'n}\right), \tag{A12}$$

$$(H_1)_{m'n'mn}=\frac{m^2\pi^2}{4}\delta_{m'm}J^4_{n'n}+m^2\pi^2 \times(K^2_{m'-m}-K^2_{m'+m})J^5_{n'n}, \quad \text{(A13)}$$

$$(H_2)_{m'n'mn}=m\pi(K^1_{m'+m}+K^1_{m'-m})(-J^5_{n'n}+2n\pi J^2_{n'n}), \quad \text{(A14)}$$

$$(H_3)_{m'n'mn}=m\pi(K^1_{m'+m}+K^1_{m'-m})(J^3_{n'n}-2J^5_{n'n}), \quad \text{(A15)}$$

where the integrals are defined below:

$$K^1_n=\int_{-1/2}^{1/2}du u\sin\left[n\pi\left(u+\frac{1}{2}\right)\right], \quad \text{(A16)}$$

$$K^2_n=\int_{-1/2}^{1/2}du u^2\cos\left[n\pi\left(u+\frac{1}{2}\right)\right], \quad \text{(A17)}$$

$$I^1_n=\int_0^1 dx\frac{\cos n\ \pi x}{b-a\cos(2\pi x)}, \quad \text{(A18)}$$

$$I^2_n=\int_0^1 dx\frac{\cos n\pi x}{[b-a\cos(2\pi x)]^2}, \quad \text{(A19)}$$

$$J^2_{mm'}=\int_0^1 dx\frac{2\sin(m\pi x)\cos(m'\pi x)f'(x)}{f(x)} =\pi a(I^1_{m+m'-2}-I^1_{m+m'+2}+I^1_{m-m'-2}-I^1_{m-m'+2}), \quad \text{(A20)}$$

$$J^3_{mm'}=\int_0^1 dx\frac{2\sin(m\pi x)\cos(m'\pi x)f''(x)}{f(x)} =2\pi^2 a(I^1_{m-m'+2}+I^1_{m-m'-2} -I^1_{m+m'+2}-I^1_{m+m'-2}), \quad \text{(A21)}$$

$$J^4_{mm'}=\int_0^1 dx\frac{2\sin(m\pi x)\sin(m'\pi x)}{f^2(x)} =I^2_{m-m'}-I^2_{m+m'}, \quad \text{(A22)}$$

$$J^5_{mm'}=\int_0^1 dx\frac{2\sin(m\pi x)\sin(m'\pi x)f'^2(x)}{f^2(x)} =2\pi^2a^2\left[I^2_{m-m'}-I^2_{m+m'}-\frac{1}{2}(I^2_{m-m'+4} +I^2_{m-m'-4}-I^2_{m+m'+4}-I^2_{m+m'-4})\right]. \quad \text{(A23)}$$

The integrals K^1_n and K^2_n in the above equations can be easily obtained:

$$K^1_n=\begin{cases}0, & \text{when } n=0\\ -\dfrac{(-1)^n+1}{2n\pi}, & \text{when } n\neq 0,\end{cases} \quad \text{(A24)}$$

$$K^2_n=\begin{cases}1/12, & \text{when } n=0\\ \dfrac{(-1)^n+1}{(n\pi)^2}, & \text{when } n\neq 0.\end{cases} \quad \text{(A25)}$$

I^1_n and I^2_n can be derived with the residue theorem. After some algebra, we have

$$I^1_n=\begin{cases}0, & \text{when } n \text{ is odd}\\ \dfrac{1}{\sqrt{b^2-a^2}}\left(b-\sqrt{\dfrac{b^2-a^2}{a}}\right)^{n/2}, & \text{when } n \text{ is even.}\end{cases} \quad \text{(A26)}$$

$$I^2_n=-\frac{\partial}{\partial b}I^1_n=\frac{b+(n/2)\sqrt{b^2-a^2}}{b^2-a^2}I^1_n. \quad \text{(A27)}$$

So, eventually every element of the Hamiltonian matrix is expressed in terms of elementary functions. This increases the computation efficiency remarkably and allows us to study large number of eigenstates of the ripple billiard. Note that similar transformations like Eq. (A3) can be applied to straighten billiards of other shapes. However, the sinusoidal boundary may be the only one where the Hamiltonian matrix elements can be calculated out exactly and expressed in terms of elementary functions.

APPENDIX B: THE HUSIMI PLOT

The Husimi plots are widely used in quantum mechanics as a counterpart to the Poincare surfaces of a section of classical systems. The Husimi distribution function [25] $H(x_0,p_{x0})$ is defined by

$$H(x_0,p_{x0})=|\langle\Psi|x_0,p_{x0}\rangle|^2, \quad \text{(B1)}$$

where $|x_0,p_{x0}\rangle$ is a coherent state that in the position basis can be represented as

$$\langle x|x_0,p_{x0}\rangle=\frac{\exp\left(-\dfrac{(x-x_0)^2}{2\sigma^2}+\dfrac{ip_0(x-x_0)}{\hbar}\right)}{(\sigma^2\pi)^{1/4}}, \quad \text{(B2)}$$

where σ is a squeezing parameter that determines the relative widths of the coherent state in the x and p directions. In our Husimi plots the position coordinate of Eq. (B1) is chosen to be the dashed line in Fig. 1 (which is basically the central vertical axis but with a small horizontal shift to avoid a zero value for states with odd parity in the horizontal direction).

[1] L. E. Reichl, *The Transition to Chaos In Conservative Classical Systems: Quantum Manifestations* (Springer-Verlag, Berlin, 1992).
[2] M. C. Gutzwiller, *Chaos in Classical and Quantum Mechanics* (Springer-Verlag, New York, 1990).
[3] E. J. Heller and S. Tomsovic, Phys. Today **46** (7), 38 (1993).
[4] E.J. Heller, Phys. Rev. Lett. **53**, 1515 (1984).
[5] G.A. Luna-Acosta, Kyungsun Na, L.E. Reichl, and A. Khrokhin Phys. Rev. E **53**, 3271 (1996).
[6] Gursoy B. Akguc and L.E. Reichl, J. Stat. Phys. **98**, 813 (2000).
[7] O. Bohigas, M. Giannoni, and Schmit, Phys. Rev. Lett. **52**, 1 (1984).
[8] F. Izrailev, Phys. Rev. Lett. **56**, 541 (1986).
[9] H.D. Graf, H.L. Harney, H. Lengeler, C.H. Lewenkopf, C. Rangacharyulu, A. Richter, P. Schardt, and H. Weidenmuller, Phys. Rev. Lett. **69**, 1296 (1992).
[10] H. Alt, C. Dembowski, H.D. Graf, R. Hofferbert, H. Rehfeld, A. Richter, and C. Schmit, Phys. Rev. E **60**, 2851 (1999).
[11] P.B. Wilkinson, T.M. Fromhold, L. Eaves, F.W. Sheard, N. Miura, and T. Takamasu, Nature (London) **380**, 608 (1996); T.M. Fromhold, P.B. Wilkinson, L. Eaves, F.W. Sheard, P.C. Main, M. Henini, M.J. Carter, N. Miura, and T. Takamasu, Chaos, Solitons Fractals **8**, 1381 (1997).
[12] V. Milner, J.L. Hanssen, W.C. Campbell, and M.G. Raizen, Phys. Rev. Lett. **86**, 1514 (2001); F.L. Moore, J.C. Robinson, C. Bharucha, P.E. Williams, and M.G. Raizen, *ibid.* **73**, 2974 (1994); N. Friedman, A. Kaplan, D. Carsso, and N. Davidson, *ibid.* **86**, 1518 (2001).
[13] T.A. Brody, J. Flores, J.B. French, P.A. Mello, A. Pandey, and S.S.M. Wong, Rev. Mod. Phys. **53**, 385 (1981); T. Terasaka and T. Matsushita, Phys. Rev. A **32**, 538 (1985).
[14] B. C. Brookes and W. F. L. Dick, *Introduction to Statistical Method* (Heinemann, London, 1969); S. L. Meyer, *Data Analysis for Scientists and Engineers* (Wiley, New York, 1975).
[15] F. Borgonovi, G. Casati, and B. Li, Phys. Rev. Lett. **77**, 4744 (1996).
[16] K.M. Frahm and D.L. Shepelyansky, Phys. Rev. Lett. **78**, 1440 (1997).
[17] E. Haller, H. Koppel, and L. Cederbaum, Chem. Phys. Lett. **101**, 215 (1983); R. Venkataraman, J. Phys. B **15**, 4293 (1982).
[18] These eigenstates fit quite well to a Bohr-Sommerfeld-like quantization condition; $kD = j(2\pi) + \phi$, where k is the wave vector, D is the length of a periodic orbit, j is expected to be an integer, and the periodic orbit associated Malsov phase ϕ is a constant, which can be obtained from the eigenenergies of periodic orbit scarred states discussed in this paper. See also Ref. [11].
[19] S. W. McDonald, Lawrence Berkeley Laboratory Report No. LBL-14837, 1983 (unpublished).
[20] S. Sridhar and E.J. Heller, Phys. Rev. A **46**, R1728 (1992).
[21] W. Chism, T. Timberlake, and L.E. Reichl, Phys. Rev. E **58**, 1713 (1998).
[22] T. Timberlake and L.E. Reichl, Phys. Rev. A **59**, 2886 (1999).
[23] F. Simonotti, E. Vergini, and M. Saraceno, Phys. Rev. E **56**, 3859 (1997).
[24] P.B. Umbanhowar, F. Melo, and H.L. Swinney, Nature (London) **382**, 793 (1996).
[25] K. Husimi, Proc. Phys. Math. Soc. Jpn. **22**, 246 (1940).